

## Research Article

Yuhong Wang, Yiwei Zhang, Zihan Jiang, Jian Wu and Chunqing Gao\*

# Mitigate the variation of energy band gap with electric field induced by quantum confinement Stark effect via a gradient quantum system for frequency-stable laser diodes

<https://doi.org/10.1515/nanoph-2025-0380>

Received August 14, 2025; accepted November 26, 2025;

published online December 9, 2025

**Abstract:** Most light-emitting devices based on quantum-confined structures are commonly utilized as electrically injected devices. However, the electric-field-dependent energy band gap induced by the quantum confinement Stark effect (QCSE) usually hinders the realization of frequency-stable laser devices. This is because the change in the energy band gap, which also means the corresponding change in the photon energy, will result in an electric-field-dependent frequency. Here, we propose a novel approach to mitigate this electric-field-dependent variation in the energy band gap by employing a gradient quantum system. In this system, the energy band edges are inclined due to the action of the indium (In)-segregation effect. This special design can effectively weaken the changes in the band profile associated with the electric field effect and counteract the electric-field-dependent band gap variations within the active region to a certain extent. Experimental studies indicate that the energy band gap of this gradient quantum system remains almost unchanged ( $<18.9 \mu\text{eV cm}^2/\text{Å}$ ) even under a relatively strong applied electric field. Meanwhile, compared with the traditional GaAs quantum well, the efficiency improvement in the band gap stability of our nanowire–well gradient system is 64.1 % and 70.6 % for the TE and TM polarization modes, respectively, which

suggests that our proposed gradient quantum structure can significantly mitigate the electric-field-induced change in the energy band gap. This achievement is of great significance for advancing the development of high-performance frequency-stable laser devices in some advanced fields, such as quantum sensing systems and optical communications.

**Keywords:** frequency-stable laser diodes; quantum-confined Stark effect; energy band gap; indium-segregation effect

## 1 Introduction

It is well known that most of the light-emitting devices based on quantum-confined structures work under the application of an additional electric field, as the electrically injected devices [1]. However, in these devices, due to the presence of the additional vertical electric fields, the conduction and valence band edges in semiconductor active materials are inclined in the same direction, reducing the energy band gap, known as the quantum confinement Stark effect (QCSE) [2]–[9]. The electric-field-dependent energy band gap caused by the QCSE is unfavorable for the realization of frequency-stable laser devices. This is because the variation in the energy band gap in the active material with an electric field means the corresponding change in photon energy. And the variation in photon energy will result in an injection-dependent frequency. Therefore, the QCSE limits the achievement of frequency-stable laser devices. However, ultra-stable laser frequencies have served as the prerequisite behind some advanced fields, such as quantum sensing systems, optical communications, optical detection, and precise experiments [10]–[13].

In addition, since the strained II–VI and III–V compounds that served as the active materials in the optoelectronic devices can usually cover a more extensive operating wavelength range [14], [15], the strained optoelectronic devices have received widespread application in

**\*Corresponding author: Chunqing Gao**, School of Optics and Photonics, Beijing Institute of Technology, Beijing 100081, China; and Key Laboratory of Information Photonics Technology, Ministry of Industry and Information Technology, Beijing 100081, China, E-mail: gao@bit.edu.cn

**Yuhong Wang, Yiwei Zhang and Zihan Jiang**, School of Optics and Photonics, Beijing Institute of Technology, Beijing 100081, China; and Key Laboratory of Information Photonics Technology, Ministry of Industry and Information Technology, Beijing 100081, China.

<https://orcid.org/0000-0003-3430-5905> (Y. Wang)

**Jian Wu**, School of Physics, Beihang University, Beijing 102206, China. <https://orcid.org/0000-0003-3573-0989>

many areas [15]–[19]. However, a similar QCSE phenomenon also occurs in these strained material systems owing to the presence of strain-driven built-in piezoelectric polarization electric fields in these material systems [3]–[5].

Given the ubiquity of the QCSE in quantum-confined devices and the negative impacts this effect brings, which are not limited to the electric-field-dependent energy band gap, but also include inefficient radiative recombination, many efforts have been made to circumvent this effect [3], [20], [21]. Previous efforts to mitigate the influence of the QCSE have mainly focused on nitride (N)-based materials, as the spontaneous polarization fields of the polar (In)GaN materials themselves, the strain-driven piezoelectric polarization fields, and the applied external electric fields in these material systems are responsible for the QCSE [2], [3]. Based on these strained N-based materials, several specific structure designs have been proposed to minimize the QCSE including the nonpolar/semi-polar structures that aim at minimizing the spontaneous polarization fields [22]–[24], the lattice-matched AlInGaN/AlInGaN multiple quantum wells and the strain-compensated InGaN/AlGaIn quantum well designed to reduce strain-related effect impact [25], [26], as well as several quantum structures with various shapes designed by energy band engineering to comprehensively attenuate the QCSE influence driven by the built-in and external applied electric fields, such as staggered well [3], [27], triangular quantum well [28], dip-shape well [29], and trapezoidal well [21]. In addition, the employment of thinner quantum wells has previously been suggested to attenuate the QCSE, but it is generally inefficient to capture the carriers into the thin quantum wells, leading to an overall lower internal quantum efficiency [22], and thus, thinning the quantum wells to mitigate the QCSE is not recommended in high-performance optoelectronic devices. Consequently, considering the complexity in regulating the growth conditions multiple times during the preparation of these specially designed structures, the difficulty of accurately controlling the material compositions, as well as the practicability in practical applications, a kind of novel quantum structure or material system that can be obtained using simple fabrication methods and growth conditions is urgently needed in reducing the QCSE impacts to obtain mass-produced high-performance devices.

Given the above considerations, we propose and recommend a gradient quantum structure with the opposite tilt-direction for conduction and valence band edges to mitigate the electric-field-dependent variation in energy band gap induced by the QCSE. This new material structure is designed and fabricated in our previous research work and exhibits many interesting properties, such as super-gain spectra, polarization insensitivity, temperature-insensitive

energy band gap, and so on [30]–[33]. In the latest research presented here, the mitigation of the impact of vertical electric field on energy band gap variation induced by the QCSE in this special structure is observed by modulating the energy band structure utilizing the In-segregation effect. In-segregation is a strain-driven effect, and its occurrence is usually limited in material growth as a growth defect due to its altered In-contents. Here, however, the In-segregation effect is effectively utilized. The band edge tilt driven by the In-segregation effect effectively counteracts the band edge tilt caused by the electric field for the valence band in this system. The modified energy band profile in the gradient system makes the energy band gap of the active material almost invariant with the change in the electric field. The relevant analysis and discussion of the mitigation of the electric-field-dependent energy band gap in this gradient quantum system utilizing the In-segregation effect are given in the following sections.

## 2 Material structure and characterization

### 2.1 Material structure

Previous research on the mitigation of the QCSE has focused mainly on N-based materials, ignoring the fact that other strained non-(In)GaIn materials and the active materials in electrically injected devices are also troubled by the QCSE due to the strain-driven built-in piezoelectric polarization electric fields and externally applied electric fields. It is well known that high-power InGaAs-based lasers are the most representative frequency-stable laser sources. They are widely used for atomic clocks in quantum sensing systems, laser diodes in optical communications, as pumping laser sources for erbium-doped fiber amplifiers and lasers, etc. [10], [34], [35]. Ultra-stable laser frequencies are generally indispensable for these systems. To mitigate the electric-field-dependent frequency drifts induced by the QCSE for InGaAs material systems is particularly important. Therefore, the InGaAs/GaAs/GaAsP quantum structure is chosen as the vehicle in our study. Based on the uniform multiatomic steps that naturally formed on initially deposited 200 nm-thick GaAs surface at a slightly misoriented GaAs (001) substrate [36]–[38], the InGaAs nanowire–well structure is formed. The formation of this hybrid structure is completely self-assembled at a step flow growth mode, as well as the 2 nm-high nanowires (one-dimension) and 10 nm-thick well (two-dimension) are combined together through a special dimension-transition interface. In addition, a given In-content of 0.17 is applied to the initial InGaAs

material. Since the InGaAs layer is inserted between the GaAs strain-buffer layers, it will experience compressive stress induced by the lattice mismatch, resulting in the occurrence of the strain-driven In-segregation effect in this InGaAs active layer under given experimental conditions. Therefore, a certain amount of In-atoms will migrate from the bottom to the top of the InGaAs layer along the material growth direction [39]–[41], which will cause the monotonically changed In-content in both well and wires. The diagram of the In-atoms migration in the nanowire–well structure is displayed in the left schematic representation of Figure 1(a).

Additionally, the schematic illustration of the epitaxial kernel structure is illustrated in the right diagram of Figure 1(a), in which the InGaAs nanowire–well structure is sandwiched by two 2 nm-thick GaAs strain-buffer layers. The insertion of strain-buffer layers can avoid the capture of carriers by dislocations (nonradiative recombination centers) caused by the large lattice mismatches between the active layers and the barriers, affecting the radiative recombination in the active region. Beyond the strain-buffer layers are 8 nm-thick  $\text{GaAs}_{0.92}\text{P}_{0.08}$  barriers. Furthermore, the InGaAs/GaAs/GaAsP system is surrounded by 2  $\mu\text{m}$ -thick AlGaAs waveguide layers.

## 2.2 Sample fabrication

This nanowire–well sample is fabricated based on the preparation method described in our previous works by a metal–organic chemical vapor deposition (MOCVD,

aix200/4) system [30]–[33]. Trimethylindium (TMIn), trimethylgallium (TMGa), arsine ( $\text{AsH}_3$ ), phosphine ( $\text{PH}_3$ ), and trimethylaluminum (TMAI) are selected as source materials. The pressure and total flow in the reaction chamber are set to 100 mbar and  $\sim 13$  slm, respectively. Moreover, the material growth rate is fixed at  $\sim 1 \mu\text{m}/\text{h}$ , and the V/III ratio is controlled at about 50. The growth temperature is  $\sim 650^\circ\text{C}$ .

## 2.3 Structural characterizations

The nanowire–well structure is characterized utilizing a special sample with the uncovered InGaAs surface, which is fabricated under the same growth conditions by terminating its epitaxial growth process just after obtaining the complete nanowire–well layer. A three-dimensional (3D) extraction of the nanowires measured in atomic force microscopy (AFM, XE100) is displayed in Figure 1(b), from which the densely and horizontally aligned InGaAs nanowires are demonstrated. To further confirm the surface morphology of the wires, the scanning electron microscope (SEM, Zeiss gemini300) analysis is carried out. A representative top-view image of the nanowires from SEM measurement is shown in Figure 1(c), where the orderly arrangement of wires can be seen. Moreover, to reveal the morphological characteristics in the side-view of the wires, the cross-sectional transmission electron microscopy (X-TEM, JEM-2100F) technique is applied here. The triangle-like nanowire cross sections with a large top-angle and a very small base-angle are presented, as exhibited in the X-TEM image of

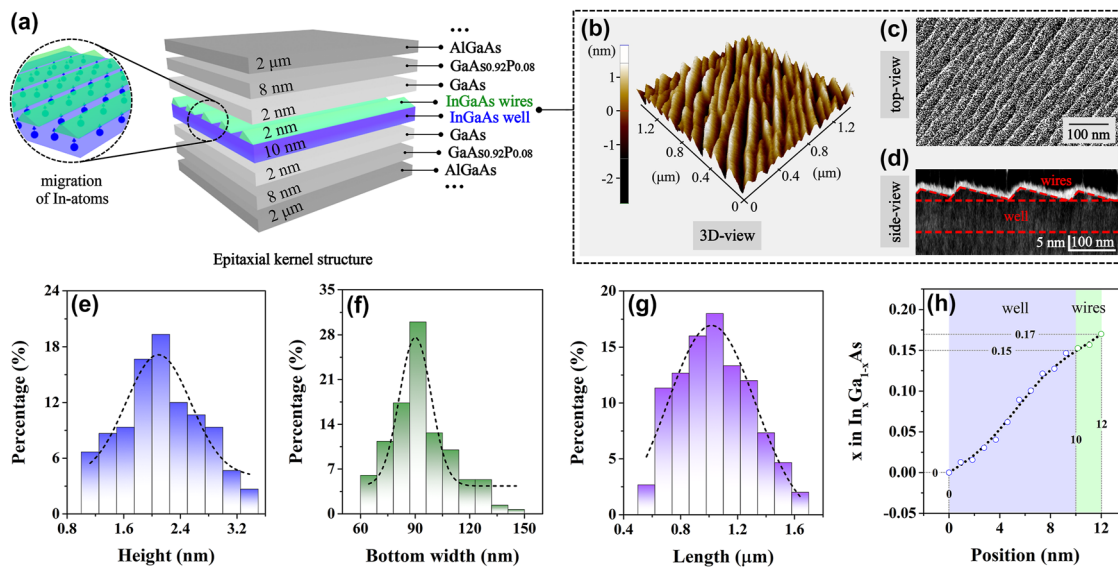


**Figure 1:** Material structure and characterization. (a) Schematic diagram of the structural characteristics of the fabricated gradient quantum structure. (b) The 3D-view, (c) top-view, and (d) side-view of on-well nanowires based on AFM, SEM, and X-TEM characterizations, respectively. Histograms of the (e) height (blue pillars), (f) bottom width (green pillars), and (g) length (purple pillars) distributions and corresponding Gaussian fitting curves (black dashed lines) of InGaAs nanowires by measuring 150 wires at random. (h) Profile of In-content in the nanowire–well structure obtained from the XPS measurement.

Figure 1(d), where the nanowire–well structure is outlined with red dashed lines. It should also be mentioned here that the white contour line along the nanowires is formed by the focused-ion-beam (FIB) treatment during the fabrication process of the sample cross section.

The statistical average height of wires is 2.0 nm, with a bottom width and length of 90.0 nm and 1.0  $\mu\text{m}$ , respectively, which are extracted by randomly measuring 150 wires in AFM images and fitting the corresponding statistical average size with a Gaussian distribution (refer to Figure 1(e)–(g)). Furthermore, since the In-content ( $x$  value) in  $\text{In}_x\text{Ga}_{1-x}\text{As}$  material can most effectively influence the energy band gap [42], the investigation of the In-content distribution in this nanowire–well structure is performed utilizing the X-ray photoelectron spectroscopy (XPS, PHI Quantera II) technology. According to the measurement result, the In-content varies approximately from  $x = 0$  to  $x = 0.15$  in the well and from  $x = 0.15$  to  $x = 0.17$  in the nanowires along the material growth direction, as is visible in Figure 1(h), which is consistent with the driving impact of the In-segregation effect. Therefore, the quantum system with gradient changes in the In-content has been achieved in our experiment, which will lead to corresponding changes in the energy band structure. The obtained structural characterizations presented here are found to be consistent with the structural information of the nanowire–well sample we prepared previously under the same fabrication conditions [30]–[33].

## 2.4 Structural division

To investigate the fundamental optical properties of the nanowire–well samples, the photoluminescence (PL) spectrum under 197 mW power injection is conducted at room temperature and depicted in Figure 2(a), in which a pump beam from an 808 nm pulsed laser (LWIRL808-40W-F) is utilized to pump the samples from the top optically. Considering the anisotropic properties

of one-dimensional nanowires, all of the PL spectra are measured along the direction parallel to the nanowires to collect the strongest light signals for a nanowire–well edge-emitting chip [38], [43]. A very obvious feature presented in the PL spectrum of Figure 2(a) is the presence of two luminescence peaks, involving energy band gaps around 1.283 eV and 1.333 eV, respectively. Given that the cross section of the nanowires presents an obtuse-triangle-like profile with a large top angle and a very small base angle, as exhibited in Figure 1(d), it is evident that the effective region of the nanowires does not completely cover the well surface, but rather presents a horizontal periodic distribution in space. Consequently, the appearance of two luminescence peaks is attributed to the contributions of the pure-well part without the nanowire coverage (marked as “well”) and the nanowire–well part with nanowire participation (marked as “wire–well”).

The schematic diagram of the structural division is displayed in Figure 2(b). Owing to the confinement of two dimensions, a larger energy band gap will form in the nanowires, compared to the well with the same material and composition but only confined by one dimension [44]. Thus, when the nanowires and the well are directly bound together, their unified energy band gap will be larger than the band gap of a pure well without a nanowire impact. As a result, the peak located at  $\sim 1.333$  eV corresponds to the nanowire–well part, and the peak near 1.283 eV is the characteristic PL peak for the pure-well part, as indicated by “wire–well” and “well” in Figure 2(a). The bi-Gaussian curve fittings for extracting the respective luminescence peaks of these two parts are also conducted and indicated in Figure 2(a), in which the luminescence peak of the nanowire–well part is represented by a green shadow, while the luminescence peak of the pure-well part corresponds to the blue shadow position. Here, the PL emission intensity from the nanowire–well part is significantly weaker than that from the pure-well part, as

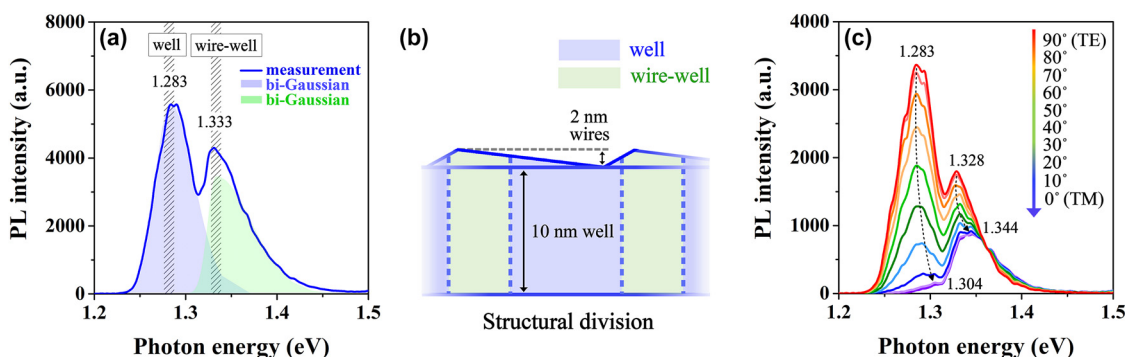


**Figure 2:** Structural division. (a) PL spectrum analysis of the nanowire–well structure with the experimental data and the bi-Gaussian fittings. (b) Schematic diagram of the structural division in the nanowire–well structure. (c) The changes in PL-peak characteristics with varying polarization from TE to TM modes in the nanowire–well structure.



observed in Figure 2(a). This intensity difference between the two luminescence peaks indicates the different proportions of these two parts in the entire active structure.

In addition, since the InGaAs well layer is inserted between the GaAs strain-buffer layers, it will experience compressive stress induced by the lattice mismatch. However, owing to the action of the wires, the tensile stress is introduced into the compressively strained quantum well via the well–wire interface, and the tensile stress counteracts part of the compressive stress in this well, so overall, the influence of the stress impact in the nanowire–well part is very weak. The related analyses have been illustrated in detail in our previous work [32]. The strain-compensated nanowire–well part designed here is aimed at weakening the influence and interference of the strain-driven built-in piezoelectric polarization electric field on the QCSE. Therefore, a more accurate mechanism of weakening the QCSE in this gradient quantum system can be considered and analyzed.

Furthermore, to confirm that the secondary peak at 1.333 eV appears in the PL spectra on account of the presence of the nanowire–well part, rather than the influence of the second energy level in the pure-well part, we measure the polarized PL spectra of this nanowire–well structure as presented in Figure 2(c). Here, the obtainment of transverse electric (TE)- and transverse magnetic (TM)-polarized spectra via rotating the polarizer from 90° to 0°, in which we define the TE polarization as the 90° polarizer angle, i.e., it takes the direction parallel to the sample surface and the TM polarization as the 0° polarizer angle, i.e., it is normal to the sample surface. The two luminescence-peak phenomena still exist when switching the polarization from TE to TM modes, and the main peak in TE polarization shifted from position ~1.283 eV to position ~1.304 eV in TM polarization, while the secondary peak shifted from position ~1.328 eV to position ~1.344 eV. More importantly, the peak located at ~1.344 eV in TM polarization has a stronger peak intensity than the peak at ~1.304 eV. Therefore, the peak at ~1.328 eV in TE mode and the peak at ~1.344 eV in TM mode are the contributions of the nanowire–well part rather than the impact of the second energy level of the pure-well part.

## 3 Results and discussions

### 3.1 Mitigated electric-field-dependent variation in energy band gap of the nanowire–well structure

To experimentally clarify the inhibitory effect of this nanowire–well gradient system on the electric-field-dependent variation in energy band gap, two different

pumping methods, electric injection and optical injection, were used to test the optical properties of these nanowire–well samples. Here, the external vertical electric field in the nanowire–well electric injection sample is applied to induce an additional QCSE in this nanowire–well structure, whereas the additional QCSE is not present in the optical injection sample. In addition, since the change in energy band gap with injection also corresponds to a change in photon energy, it will result in a change in luminescence peak position. Therefore, by comparing the luminescence peak positions of PL spectra and electroluminescence (EL) spectra, the mitigation degree of electric-field-dependent variation in the energy band gap induced by the QCSE in this structure can be judged.

The injection power-dependent unpolarized, TE-polarized, and TM-polarized PL spectra are measured in the power range of 68 mW–197 mW at room temperature and displayed in Figure 3(a)–(c). Meanwhile, the injection power-dependent unpolarized, TE-polarized, and TM-polarized EL spectra are measured in the power range of 90 mW–360 mW at room temperature and exhibited in Figure 3(d)–(f). Here, the EL spectra of the nanowire–well sample were obtained by utilizing a continuous current source (LDC220C) perpendicular to the sample surface for electrical pumping. As expected, there is no obvious shift in the peak positions of the EL spectra compared to the PL spectra at almost the same injection level. The slight fluctuations in peak positions are due to the small differences between samples from different batches. Consequently, the electric-field-dependent variation in the energy band gap can be effectively mitigated in this nanowire–well structure.

To further illustrate the suppression of the electric-field-dependent variation in energy band gap in the nanowire–well gradient quantum system, the unpolarized, TE-polarized, and TM-polarized EL spectra of the nanowire–well structure at room temperature with a large injection current density range from 7 A/cm<sup>2</sup> to 60 A/cm<sup>2</sup> are measured, as shown in Figure 4(a)–(c). In addition, a traditional GaAs quantum well, as a reference structure, has been studied for its energy band gap variation with the electric field, as displayed in Figure 4(d)–(f). For the nanowire–well gradient quantum system, there is no obvious shift in the luminescence peak of the EL spectra with the gradually increased injection. Even at high current injection, that is, under the action of a strong electric field, the structure should theoretically be affected by a strong QCSE effect, so the luminescence peak should have a very obvious shift, but it does not appear in our experiment. Specifically, the energy band gap changes of the pure-well part and the nanowire–well part are both <1.0 meV for the unpolarized EL spectra of the nanowire–well system

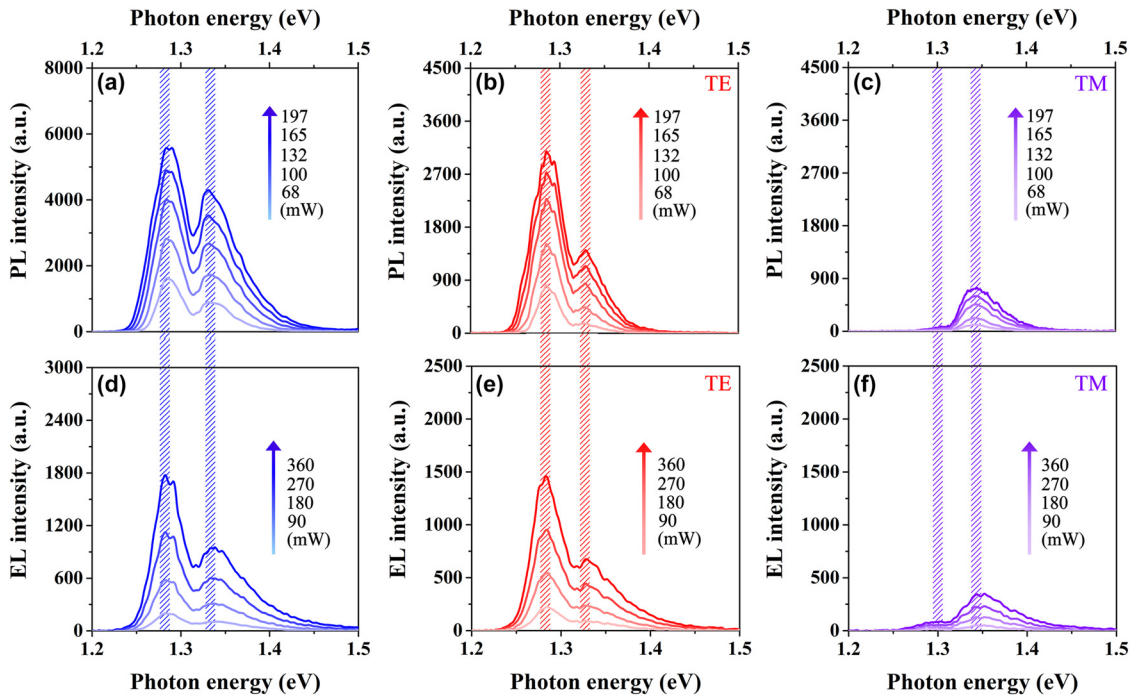


**Figure 3:** Luminescence peak characterizations of the PL and the EL spectra at similar injection. Injection power-dependent (a) unpolarized, (b) TE-polarized, and (c) TM-polarized PL spectra of the nanowire–well structure from 68 mW to 197 mW at room temperature. Injection power-dependent (d) unpolarized, (e) TE-polarized, and (f) TM-polarized EL spectra of the nanowire–well structure from 90 mW to 360 mW at room temperature.

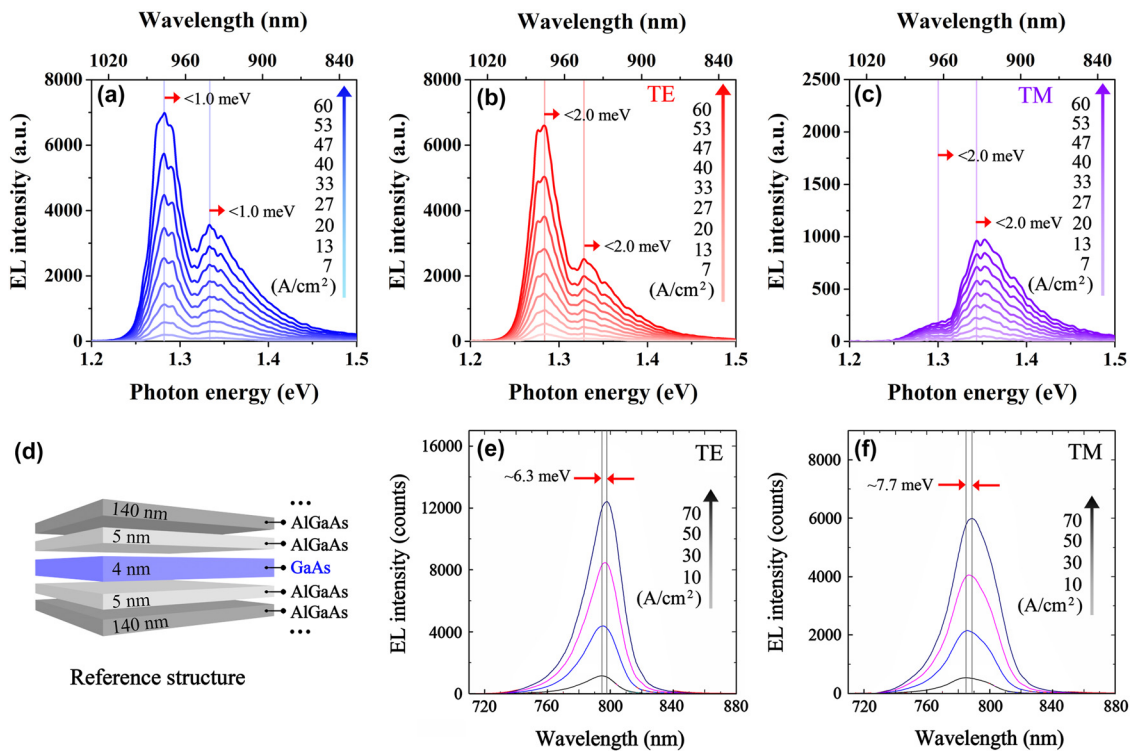


**Figure 4:** Luminescence peak characterizations of the EL spectra in the nanowire–well structure and the GaAs reference quantum well at similar injection. (a) Unpolarized, (b) TE-polarized, and (c) TM-polarized EL spectra of the nanowire–well structure at room temperature with the injection current density from 7 A/cm<sup>2</sup> to 60 A/cm<sup>2</sup>. (d) Schematic diagram of the structure composition of the GaAs reference quantum well. (e) TE-polarized and (f) TM-polarized EL spectra of the GaAs reference quantum well at room temperature with current density increasing from 10 A/cm<sup>2</sup> to 70 A/cm<sup>2</sup> [45].

with an injection current density range from 7 A/cm<sup>2</sup> to 60 A/cm<sup>2</sup>. For the TE- and TM-polarized EL spectra of the nanowire–well system, the energy band gap changes are both <2.0 meV. The change rate of the energy band gap with injection current in the nanowire–well gradient system is <18.9  $\mu\text{eV cm}^2/\text{A}$  for the unpolarized property. For the TE and TM polarization modes, the sensitivity to current injection is <37.7  $\mu\text{eV cm}^2/\text{A}$ . Due to the lack of an In-segregation effect, the GaAs quantum well, as a traditional quantum system rather than a gradient quantum system, is used as a reference structure. The schematic diagram of the epitaxial kernel structure of the GaAs quantum well is shown in Figure 4(d). The active material is a 4 nm-thick unstrained GaAs single quantum well, which is sandwiched by 5 nm-thick Al<sub>0.25</sub>Ga<sub>0.75</sub>As barrier layers [45]. The TE- and TM-polarized EL spectra of the GaAs quantum well are measured under a continuous current source (LDC210C) in a current density range of 10 A/cm<sup>2</sup>–70 A/cm<sup>2</sup> at room temperature, as shown in Figure 4(e) and (f) [45]. After measurement, within the range of current density variation, for the GaAs quantum well, the changes in band gap under TE and TM polarization modes are  $\sim 6.3$  meV and  $\sim 7.7$  meV, respectively. Correspondingly, the change rates of band gap are  $\sim 105.0$   $\mu\text{eV cm}^2/\text{A}$  and  $\sim 128.3$   $\mu\text{eV cm}^2/\text{A}$ . Here, we define the efficiency improvement in the band gap stability ( $\eta$ ) of the nanowire–well gradient system compared to the GaAs quantum well as:

$$\eta = \left| \frac{R_{\text{WW}} - R_{\text{GaAs}}}{R_{\text{GaAs}}} \right| \times 100 \% \quad (1)$$

where  $R_{\text{WW}}$  and  $R_{\text{GaAs}}$  represent the change rates of energy band gap in the nanowire–well gradient system and GaAs quantum well, respectively. Therefore, compared with the GaAs well, a traditional quantum system, the efficiency improvement in the band gap stability of the nanowire–well gradient system is 64.1 % and 70.6 % for the TE polarization and TM polarization, respectively. Studies have shown that using a thinner active layer can further weaken the QCSE [22], [46]. The standard treatment of the QCSE in a quantum well based on time-independent perturbation theory predicts that, to leading order, the energy band gap shift in a fixed electric field strength varies as the fourth power of the quantum well thickness. Therefore, compared to the 12 nm-thick nanowire–well layer, the QCSE in the thinner GaAs quantum well layer (4 nm thick) should be more strongly suppressed. However, the QCSE has been further suppressed in the nanowire–well gradient system, and the energy band gap stability has been greatly improved compared to that of the GaAs well. By comparing the energy band gap variation of the nanowire–well sample injected

with light and that injected with electricity, as well as comparing the energy band gap variation of the electrically injected nanowire–well sample and the electrically injected GaAs quantum well sample, the band gap changes induced by QCSE in nanowire–well gradient quantum systems are effectively mitigated.

In addition, as a typical GaAs/In<sub>0.17</sub>Ga<sub>0.83</sub>As/GaAs material system, the large lattice constant between these two materials will induce significant compressive stress in the pure InGaAs quantum well. In order to weaken the influence and interference of the strain-driven built-in piezoelectric polarization electric field on the QCSE and more accurately consider the mechanism of mitigating the QCSE in our specially designed gradient quantum system based on energy band engineering, the nanowire–well part in the nanowire–well structure is designed. In the nanowire–well part, due to the gradual increase of In-content along the growth direction, the lattice of the nanowires is larger than that of the quantum well, so the well is subjected to the tensile stress from the nanowires. Therefore, the tensile stress is introduced into the compressively strained quantum well, and the tensile stress counteracts part of the compressive stress in this well; thus, the influence of the stress impact in the nanowire–well part is very weak. These related explanations have been illustrated in detail in the previous work [32].

To clarify this weak stress effect in the nanowire–well part, the TE- and TM-polarized PL fitting spectra of the nanowire–well part are displayed in Figure 5(a), as well as the integrated PL intensities of the TE- and TM-polarized PL spectra in this part are illustrated in Figure 5(b). Meanwhile, for comparison, the TE- and TM-polarized PL fitting spectra of the pure-well part are exhibited in Figure 5(c), as well as the integrated PL intensities of the TE- and TM-polarized PL spectra in this part are illustrated in Figure 5(d). It is very obvious that there is only a very small difference in the spectral intensity of TE and TM polarization modes in the nanowire–well part, but this difference is very large in the pure-well part. The degree of polarization (DOP), defined as  $\text{DOP} = (I_{\text{TE}} - I_{\text{TM}})/(I_{\text{TE}} + I_{\text{TM}})$  [47]–[49], is usually used to reflect the strain strength in the structure. Here,  $I_{\text{TE}}$  and  $I_{\text{TM}}$  denote the integrated PL intensities of TE polarization and TM polarization, respectively. With the data in Figure 5(b) and (d), the calculated DOP values are 0.09 and 0.97 for the emissions from the nanowire–well part and the pure-well part, respectively. The very low DOP indicates the comparable TE and TM intensities in the nanowire–well part, suggesting that the stress action in this part is very weak, and this part is close to a no-strain part. Therefore, the strain-driven built-in piezoelectric polarization electric

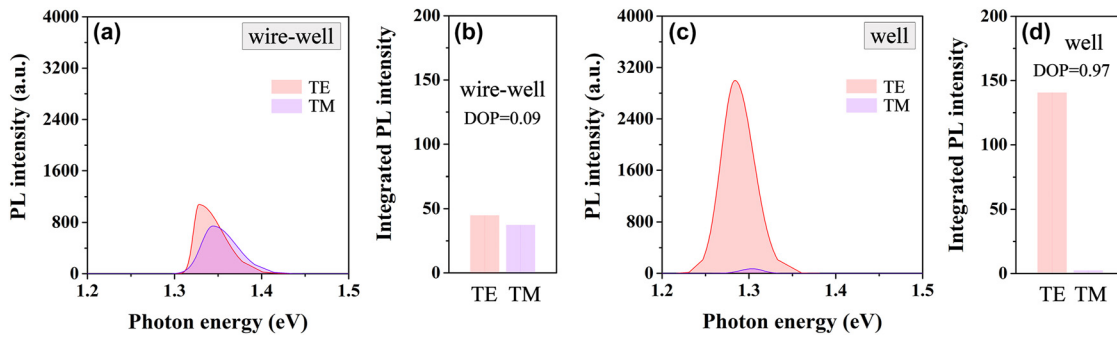


**Figure 5:** Polarization characteristics of the nanowire-well part and the pure-well part. (a) TE- and TM-polarized PL spectra of the nanowire-well part in the nanowire-well structure. (b) The integrated PL intensities of the TE- and TM-polarized PL spectra in the nanowire-well part. (c) The polarized PL spectra of the pure-well part in the nanowire-well structure. (d) The integrated PL intensities of the polarized PL spectra in the pure-well part.

field is extremely weak in this nanowire-well part. Thus, when an additional electric field is applied to this system through external devices, there is no interference from the built-in electric field. It also eliminates the possibility that the built-in electric field and the external electric field have opposite directions, resulting in the cancellation of the electric field strength acting on the active region of the sample. Therefore, temporarily, it can be considered that when the nanowire-well part serves as the investigation target, the mitigation mechanism of this gradient nanowire-well

structure on the energy band gap variation induced by QCSE can be analyzed more clearly.

To distinguish the luminescence peaks of the pure-well part and the nanowire-well part from the nanowire-well sample, the EL spectra of the nanowire-well sample are fitted by bi-Gaussian fitting. The injection current density-dependent unpolarized, TE-, and TM-polarized EL fitted spectra of the pure-well part are shown in Figure 6(a)–(c), as well as the injection current density-dependent unpolarized, TE-, and TM-polarized EL fitted spectra of the

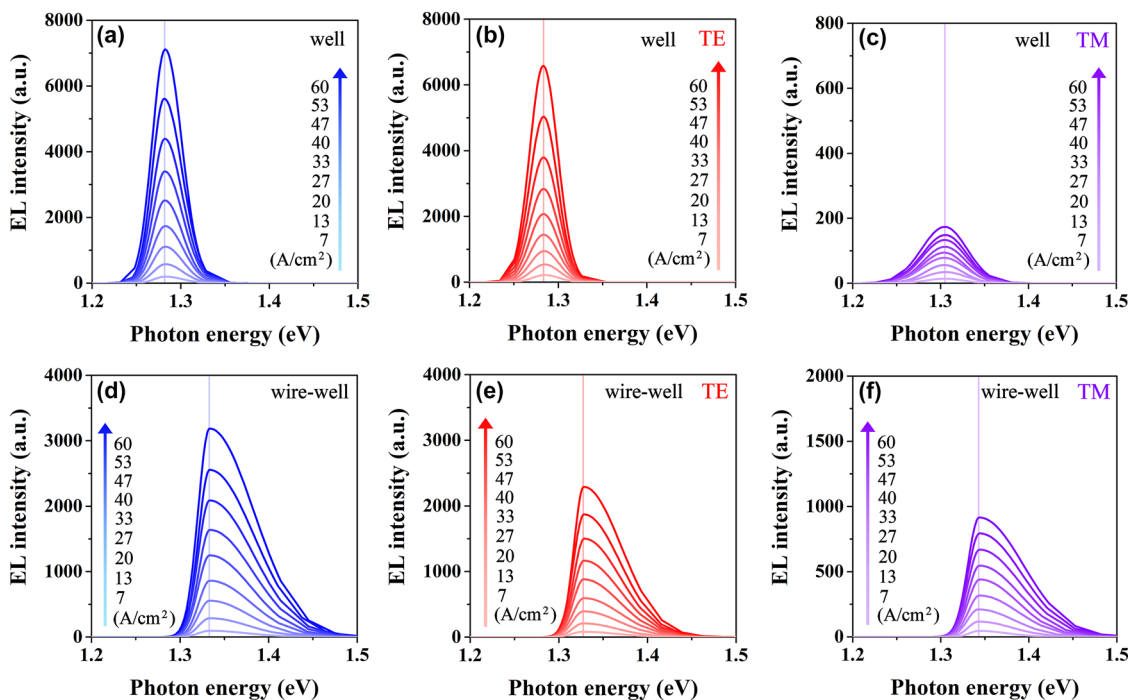


**Figure 6:** Luminescence peak characterizations of the EL fitted spectra in the pure-well part and the nanowire-well part at similar injection. (a) Unpolarized, (b) TE-polarized, and (c) TM-polarized EL fitted spectra of the pure-well part at room temperature with injection current density increasing from 7 A/cm<sup>2</sup> to 60 A/cm<sup>2</sup>. (d) Unpolarized, (e) TE-polarized, and (f) TM-polarized EL fitted spectra of the nanowire-well part at room temperature with injection current density increasing from 7 A/cm<sup>2</sup> to 60 A/cm<sup>2</sup>.



nanowire–well part are depicted in Figure 6(d)–(f), respectively. There is no obvious change in the energy band gap, not only for the pure-well part with a built-in electric field but also for the nanowire–well part without a built-in electric field.

The electric-field-independent energy band gap is obtained in both the nanowire–well part and the pure-well part, which indicates that the mechanism of mitigating the variation of energy band gap with electric field induced by the QCSE can target both strain-driven built-in piezoelectric polarization electric fields as well as external electric fields under electrical injection. Utilizing the In-segregation effect, based on the energy band engineering, the electric-field-independent energy band gap is obtained in this InGaAs nanowire–well structure, which provides a new idea for the realization of frequency-stable laser devices and other high-performance optoelectronic devices.

### 3.2 Mechanism of mitigating electric-field-dependent energy band gap variation

To illustrate the mitigation mechanism of the nanowire–well structure on the electric-field-dependent energy band gap variation induced by the QCSE, the energy

band together with electron and hole wave function diagrams of an ideal  $\text{In}_{0.17}\text{Ga}_{0.83}\text{As}$  quantum well without electric field and stress impacts as well as a strained  $\text{In}_{0.17}\text{Ga}_{0.83}\text{As}$  quantum well with a vertical external applied electric field are drawn and presented in Figure 7(a) and (b), respectively. The energy band edges in the unstrained well of Figure 7(a) are flat due to the absence of the electric field impact, but in the quantum well with the external applied electric field and stress impacts, as exhibited in Figure 7(b), the conduction band (denoted as  $C$  in the figure) and valence band (denoted as  $V$  in the figure) edges are inclined and tilt in the same direction. This tilt of band edges induced by electric fields makes the energy band gap of the active material decrease compared to the ideal well without the electric field impact in Figure 7(a).

To mitigate electric-field-dependent energy band gap variation induced by the QCSE, we propose a gradient quantum system that features a design of continuously increased In-content along the material growth direction based on the In-segregation effect. Here, the pure-well part of the nanowire–well structure is selected as an example for the following analyses. The energy band structure diagram of the pure-well part is illustrated in Figure 7(c). It could be found that the conduction ( $C$ ) and valence ( $V$ ) band edges in this system tilt in different directions due to the

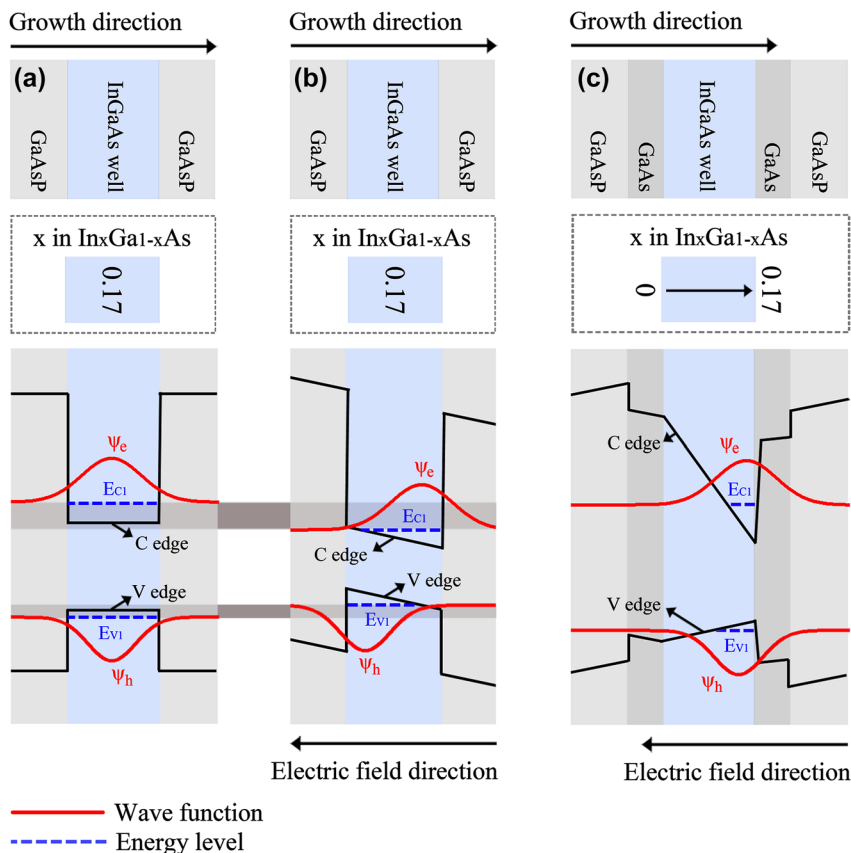


**Figure 7:** Mechanism of mitigating electric-field-dependent energy band gap variation. Schematic representation of the kernel epitaxial structure, In-content in InGaAs active layer, and energy band structure in (a) an ideal InGaAs quantum well without electric field and stress impacts, (b) a strained InGaAs quantum well with an external applied electric field, and (c) the pure-well part in the nanowire–well structure with an external applied electric field.

continuously increased In-content along the material growth direction. Furthermore, for the valence band in this system, the band edge tilt caused by the In-segregation effect and the band edge tilt caused by the electric field are in two opposite directions, so this special design of gradient In-content can compensate for the valence band tilt caused by the electric field to some extent. Therefore, this modified energy band profile in the gradient quantum system makes the energy band gap of the active material almost invariant with the change in the electric field. So the electric-field-dependent energy band gap variation can be effectively mitigated, which provides a feasible way to develop frequency-stable laser diodes and increase their practical value.

## 4 Conclusions

In summary, a method for mitigating the electric-field-dependent energy band gap variation induced by the QCSE based on the nanowire–well structure with a gradient In-content is introduced in this paper. In this special structure, the energy band profile is modified by the In-segregation effect, which effectively mitigates the variation of the energy band gap with the electric field to some extent. Experimental results indicate that the energy band gap of the active material remains relatively stable at the identical injection level in both electric injection samples that are subjected to the vertical electric field and in the optical injection samples without the electric field impact. Meanwhile, as the external electric field is gradually increased, there is also no obvious change in the energy band gap in the electric injection samples. Importantly, compared with a thinner GaAs reference quantum well that theoretically has a stronger weakening effect on the QCSE, the nanowire–well gradient system exhibits stronger band gap stability and a higher band gap stability efficiency. This realization of electric-field-independent energy band gap in the InGaAs nanowire–well gradient system brings a new opportunity for the realization of frequency-stable laser diodes and enhances the application value of quantum-confined optoelectronic devices.

**Research funding:** None declared.

**Author contributions:** All authors have accepted responsibility for the entire content of this manuscript and consented to its submission to the journal, reviewed all the results, and approved the final version of the manuscript. YW: writing, concept, execution. YZ: data acquisition. ZJ: analysis. JW: critical revision. CG: guidance, critical revision.

**Conflict of interest:** Authors state no conflict of interest.

**Data availability:** The datasets generated during the current study are available from the corresponding author upon reasonable request.

## References

- [1] A. M. Miteva, S. J. Vlaev, V. T. Donchev, and L. M. Gaggero-Sager, “Quantum confined Stark effect in n-type delta-doped quantum wells,” *Rev. Mex. Fis. S.*, vol. 53, no. 7, pp. 74–77, 2007.
- [2] A. J. Moseley, D. J. Robbins, A. C. Marshall, M. Q. Kearley, and J. I. Davies, “Quantum confined Stark effect in InGaAs/InP single quantum wells investigated by photocurrent spectroscopy,” *Semicond. Sci. Technol.*, vol. 4, no. 3, pp. 184–190, 1989.
- [3] M. Zhang *et al.*, “Performance improvement of AlGaN-based deep ultraviolet optoelectronic diodes by using staggered quantum wells,” *Superlattices Microstruct.*, vol. 75, pp. 63–71, 2014.
- [4] H. R. Alaei and H. Eshghi, “Theoretical modeling for quantum-confined Stark effect due to internal piezoelectric fields in GaInN strained quantum wells,” *Phys. Lett. A*, vol. 374, no. 1, pp. 66–69, 2009.
- [5] X. L. Xu *et al.*, “Enhanced localisation effect and reduced quantum-confined Stark effect of carriers in InGaN/GaN multiple quantum wells embedded in nanopillars,” *J. Lumin.*, vol. 203, pp. 216–221, 2018.
- [6] A. Pandey *et al.*, “Strain-engineered N-polar InGaN nanowires towards high-efficiency red LEDs on the micrometer scale,” *Photonics Res.*, vol. 10, no. 12, pp. 2809–2815, 2022.
- [7] O. Schilling, A. Forchel, A. Kohl, and S. Brittner, “Optical analysis of quantum confined Stark effect in overgrown InGaAs/InP quantum wires,” *J. Vac. Sci. Technol. B*, vol. 11, no. 6, pp. 2556–2559, 1993.
- [8] C. Li, Z. Ji, J. Li, M. Xu, H. Xiao, and X. Xu, “Electroluminescence properties of InGaN/GaN multiple quantum well-based LEDs with different indium contents and different well widths,” *Sci. Rep.*, vol. 7, no. 1, 2017, Art. no. 15301.
- [9] P. Steinmann, B. Borchert, and B. Stegmüller, “Asymmetric quantum wells with enhanced QCSE: Modulation behaviour and application for integrated laser/modulator,” *IEEE Photonics Technol. Lett.*, vol. 9, no. 2, pp. 191–193, 1997.
- [10] J. W. Zhang *et al.*, “High-temperature operating 894.6 nm-VCSELs with extremely low threshold for Cs-based chip scale atomic clocks,” *Opt. Express*, vol. 23, no. 11, pp. 14763–14773, 2015.
- [11] W. Loh, *et al.*, “Operation of an optical atomic clock with a Brillouin laser subsystem,” *Nature*, vol. 588, no. 7837, pp. 244–249, 2020.
- [12] Y. D. Tan, J. J. Chen, Y. Zhou, C. F. Cheng, and S. M. Hu, “Frequency-stabilized mid-infrared laser source for precision spectroscopy,” *Chin. J. Chem. Phys.*, vol. 37, no. 2, pp. 147–152, 2024.
- [13] I. Coddington, W. C. Swann, L. Nenadovic, and N. R. Newbury, “Rapid and precise absolute distance measurements at long range,” *Nat. Photonics*, vol. 3, pp. 351–356, 2009.
- [14] K. Park *et al.*, “Vertical profiling of ultrafast carrier dynamics in partially strain relaxed and strained InGaN grown on GaN/sapphire template of different in composition,” *Appl. Surf. Sci.*, vol. 608, 2023, Art. no. 155020.

- [15] A. Kumari and R. K. Mishra, "Temperature dependence of optical gain in compressively strained InAsP/GaInAs based quantum well heterostructure for short wavelength infrared applications," *Phys. B*, vol. 677, 2024, Art. no. 415701.
- [16] Y. C. Wang, J. Yang, F. Liang, Z. S. Liu, and D. G. Zhao, "Strain control and its effect on the optical properties of InGa<sub>N</sub>/Ga<sub>N</sub> multiple quantum wells," *J. Lumin.*, vol. 266, 2024, Art. no. 120335.
- [17] H. J. Yang *et al.*, "The enhanced photo absorption and carrier transportation of InGa<sub>N</sub>/Ga<sub>N</sub> quantum wells for photodiode detector applications," *Sci. Rep.*, vol. 7, 2017, Art. no. 43357.
- [18] K. Sarkar, P. Devi, K. Kim, and P. Kumar, "III–V nanowire-based ultraviolet to terahertz photodetectors: Device strategies, recent developments, and future possibilities," *Trends Anal. Chem.*, vol. 130, 2020, Art. no. 115989.
- [19] A. Kumari and R. K. Mishra, "Comparative study of optical characteristics of SQW and DQWs InGaAs/GaAsSb/AlAsSb based compressively strained heterostructures," *Micro Nanostruct.*, vol. 175, 2023, Art. no. 207505.
- [20] A. A. Ronald, E. Yik-Khoon, and T. Nelson, "Polarization engineering via staggered InGa<sub>N</sub> quantum wells for radiative efficiency enhancement of light emitting diodes," *Appl. Phys. Lett.*, vol. 91, no. 9, 2007, Art. no. 091110.
- [21] S. H. Han *et al.*, "Improvement of efficiency droop in InGa<sub>N</sub>/Ga<sub>N</sub> multiple quantum well light-emitting diodes with trapezoidal wells," *J. Phys. D: Appl. Phys.*, vol. 43, 2010, Art. no. 354004.
- [22] J. P. Liu *et al.*, "Blue light emitting diodes grown on freestanding (11-20) a-plane Ga<sub>N</sub> substrates," *Appl. Phys. Lett.*, vol. 92, no. 1, 2008, Art. no. 011123.
- [23] S. C. Ling, T. C. Lu, S. P. Chang, J. R. Chen, H. C. Kuo, and S. C. Wang, "Low efficiency droop in blue-green m-plane InGa<sub>N</sub>/Ga<sub>N</sub> light emitting diodes," *Appl. Phys. Lett.*, vol. 96, no. 23, 2010, Art. no. 231101.
- [24] H. Yu, L. K. Lee, T. Jung, and P. C. Ku, "Photoluminescence study of semipolar {101} InGa<sub>N</sub>/Ga<sub>N</sub> multiple quantum wells grown by selective area epitaxy," *Appl. Phys. Lett.*, vol. 90, no. 14, 2007, Art. no. 141906.
- [25] M. Shatalov *et al.*, "Deep ultraviolet light-emitting diodes using quaternary AlInGa<sub>N</sub> multiple quantum wells," *IEEE J. Sel. Top. Quantum Electron.*, vol. 8, no. 2, pp. 302–309, 2002.
- [26] H. Zhao, R. A. Arif, Y. K. Ee, and N. Tansu, "Optical gain analysis of strain-compensated InGa<sub>N</sub>-AlGa<sub>N</sub> quantum well active regions for lasers emitting at 420–500 nm," *Opt. Quantum Electron.*, vol. 40, no. 5, pp. 301–306, 2008.
- [27] X. Y. Zhao, B. Tang, L. Y. Gong, J. C. Bai, J. F. Ping, and S. J. Zhou, "Rational construction of staggered InGa<sub>N</sub> quantum wells for efficient yellow optoelectronic diodes," *Appl. Phys. Lett.*, vol. 118, no. 18, 2021, Art. no. 182102.
- [28] R. J. Choi, Y. B. Hahn, H. W. Shim, M. S. Han, E. K. Suh, and H. J. Lee, "Fabrication of efficient blue optoelectronic diodes with InGa<sub>N</sub>/Ga<sub>N</sub> triangular multiple quantum wells," *Appl. Phys. Lett.*, vol. 82, no. 17, p. 2764, 2003.
- [29] S. H. Park, D. Ahn, B. H. Koo, and J. W. Kim, "Dip-shaped InGa<sub>N</sub>/Ga<sub>N</sub> quantum-well optoelectronic diodes with high efficiency," *Appl. Phys. Lett.*, vol. 95, no. 6, 2009, Art. no. 063507.
- [30] Y. H. Wang *et al.*, "Super-gain nanostructure with self-assembled well-wire complex energy-band engineering for high performance of tunable laser diodes," *Nanophotonics*, vol. 12, no. 9, pp. 1763–1776, 2023.
- [31] H. X. Tai, *et al.*, "Directly-coupled well-wire hybrid quantum confinement lasers with the enhanced high temperature performance," *J. Phys. D: Appl. Phys.*, vol. 56, no. 23, p. 23LT01, 2023.
- [32] Y. H. Wang, *et al.*, "Ultra-broadband depolarization based on directly-coupled quantum wire-to-well modulation and their aliasing effect for polarization-insensitive light-emitting diodes," *Nanoscale*, vol. 15, no. 44, pp. 18044–18052, 2023.
- [33] Y. H. Wang, *et al.*, "Realization of temperature-insensitive energy band-gap based on nanowire-well quantum systems for thermally frequency-stable laser diodes," *J. Mater. Chem. C*, vol. 12, no. 17, pp. 6161–6169, 2024.
- [34] L. J. Mawst *et al.*, "High-power, single-mode, Al-free InGaAs(P)/InGaP/GaAs distributed feedback diode lasers," *J. Cryst. Growth*, vol. 195, nos. 1–4, pp. 609–616, 1998.
- [35] A. Orth, J. P. Reithmaier, R. Zeh, H. Doleschel, and A. Forchel, "First order gain-coupled GaInAs/GaAs distributed feedback laser diodes patterned by focused ion beam implantation," *Appl. Phys. Lett.*, vol. 69, no. 13, pp. 1906–1908, 1996.
- [36] S. Lee, M. Akabori, T. Shirahata, K. Takada, J. Motohisa, and T. Fukui, "The initial stage of InGaAs growth by MOVPE on multiaxial-stepped GaAs structures," *J. Cryst. Growth*, vol. 231, nos. 1–2, pp. 75–81, 2001.
- [37] J. Ishizaki, S. Goto, M. Kishida, T. Fukui, and H. Hasegawa, "Mechanism of multiaxial step formation during metalorganic chemical vapor deposition growth of GaAs on (001) vicinal surface studied by atomic force microscopy," *Jpn. J. Appl. Phys.*, vol. 33, no. 15, pp. 721–726, 1994.
- [38] S. Hara, J. Motohisa, T. Fukui, and H. Hasegawa, "Quantum well wire fabrication method using self-organized multiaxial steps on vicinal (001) GaAs surfaces by metalorganic vapor phase epitaxy," *Jpn. J. Appl. Phys.*, vol. 34, no. 85, pp. 4401–4404, 1995.
- [39] S. Martini, J. E. Manzoli, and A. A. Quivy, "Study of the influence of indium segregation on the optical properties of InGaAs/GaAs quantum wells via split-operator method," *J. Vac. Sci. Technol. B*, vol. 28, no. 2, pp. 277–283, 2010.
- [40] S. Martini, *et al.*, "Ex-situ investigation of indium segregation in InGaAs/GaAs quantum wells using high-resolution X-ray diffraction," *J. Appl. Phys.*, vol. 94, no. 11, pp. 7050–7052, 2003.
- [41] A. S. Sozykin, S. S. Strelchenko, E. V. Prokolkin, and M. A. Ladugin, "Thermodynamics and kinetics of indium segregation in InGaAs/GaAs heterostructures grown by MOCVD," *J. Cryst. Growth*, vol. 363, pp. 253–257, 2013.
- [42] W. M. Zhou, H. Shen, J. Pamulapati, P. Cooke, and M. Dutta, "Heavy- and light-hole band crossing in a variable-strain quantum-well heterostructure," *Phys. Rev. B*, vol. 51, no. 8, pp. 5461–5464, 1995.
- [43] S. Keller, N. Pfaff, S. P. DenBaars, and U. K. Mishra, "Polarization spectroscopy of N-polar AlGa<sub>N</sub>/Ga<sub>N</sub> multi quantum wells grown on vicinal (0001) Ga<sub>N</sub>," *Appl. Phys. Lett.*, vol. 101, no. 18, 2012, Art. no. 182103.
- [44] M. Asada, Y. Miyamoto, and Y. Suematsu, "Gain and the threshold of three-dimensional quantum-box lasers," *IEEE J. Quantum Electron.*, vol. 22, no. 9, pp. 1915–1921, 1986.
- [45] M. L. Ma *et al.*, "Measurement of gain characteristics of semiconductor lasers by amplified spontaneous emissions from dual facets," *Opt. Express*, vol. 21, no. 8, pp. 10335–10341, 2013.

- [46] M. Tommy, A. B. Christopher, H. P. Frank, and E. P. O'Reilly, "Lateral quantum-confined stark effect for integrated quantum dot electroabsorption modulators," *IEEE J. Sel. Top. Quantum Electron.*, vol. 31, no. 5, 2025, Art. no. 1900310.
- [47] M. Shan *et al.*, "Deep UV laser at 249 nm based on GaN quantum wells," *ACS Photonics*, vol. 6, no. 10, pp. 2387–2391, 2019.
- [48] P. Jayavel, *et al.*, "Optical polarization properties of InAs/GaAs quantum dot semiconductor optical amplifier," *Jpn. J. Appl. Phys.*, vol. 44, no. 45, pp. 2528–2530, 2005.
- [49] J. Liu *et al.*, "InGaN-based quantum well superluminescent diode monolithically grown on Si," *ACS Photonics*, vol. 6, no. 8, pp. 2104–2109.